Chromatic Aberration Correction for Improved Stimulated Raman Signal

Peter Bagdovitz

A thesis

submitted in partial fulfillment of the

requirements for the degree of

Master of Science in Applied Chemical Science and Technology

University of Washington

2026

Committee:

Dan Fu

Jiaojian Shi

Program Authorized to Offer Degree:

Chemistry

University of Washington

Abstract

Chromatic Aberration Correction for Improved Stimulated Raman Signal

Peter Bagdovitz

Chair of the Supervisory Committee:

Dan Fu

Department Of Chemistry

Stimulated Raman scattering (SRS) microscopy enables label-free chemical imaging by exploiting the vibrational signatures of molecular bonds, but signal intensity degrades significantly at large field angles due to chromatic aberration in the microscope system.[1] This work develops a quantitative characterization pipeline for measuring chromatic focal shift and lateral color aberration across the field of view, using Z-stack imaging of a calibration grid target analyzed in Python. The pipeline was validated by demonstrating its sensitivity to known differences in optical performance between a single achromatic doublet and a Plössl eyepiece configuration. A systematic comparison of over twenty commercial lens configurations was conducted in Zemax OpticStudio, using

chromatic focal shift and lateral color as optimization targets. A Plössl eyepiece consisting of two Newport Scientific PAC12AR.16 100 mm achromatic doublets was identified as the strongest candidate for lateral color correction. Experimental validation confirmed the simulation results, with the Newport configuration reducing average lateral color to sub pixel levels at high field angles and producing substantially increased SRS signal uniformity across the field of view compared to the baseline Thorlabs configuration. These results demonstrate that careful optical characterization and commercial lens selection can meaningfully improve SRS microscope performance without requiring custom optics.

List of Figures

Figure **2.5** A 2D scatter plot of the peak positions of the derivative profiles across the 100x100 lines drawn on the grid image. Where X and Y axes are the peak position, and color is the Z depth of the frame.

Figure **2.6** A line plot of chromatic focal shift in microns vs wavelength in nanometers.

Figure **2.7** A 2D scatterplot of the grid intersections from the 1030 nm image and 793 nm image overlaid.

Figure **2.9** A layout diagram of the scan lens tube lens and objective microscope system in Zemax OpticStudio

Figure **2.10** Three Plössl eyepieces with incident rays traced.

Figure **3.1 (A)** A 2D scatterplot of the grid intersections from the Thorlabs Plössl eyepiece 1030 nm image and 793 nm image overlaid.

Figure **3.1 (B)** A 2D scatterplot of the grid intersections from the Thorlabs Achromat 1030 nm image and 793 nm image overlaid.

Figure **3.2** Line plots of aberration metrics for a Thorlabs AC-254-50-B Scan Lens.

Figure **3.3** A 2D scatterplot of the grid intersections from the Newport Scientific Plössl eyepiece 1030 nm image and 793 nm image overlaid.

Figure **3.4** Line plots of aberration metrics for a Newport Scientific Plössl eyepiece compared with a Thorlabs Plössl eyepiece and Thorlabs achromatic doublet.

Figure **3.5** A comparison of SRS images taken with the Thorlabs Scan Lens and Newport Scan Lens

Acknowledgements

I would like to thank the members of my group for helping me so much throughout my two years in this program. Murdoch for introduction and mentorship in the lab. Brian Wong for begrudgingly teaching me many important skills. King Wai Chiu and Erin Dunnington for close guidance on SRS procedures and fun times together. Danielle Sorg for being my closest lab mate and peer. Sarah Ransom for the many snacks and helpful chats and Chisa Zensho and Jon Kim for all the great conversations and advice. Finally thank you to Dan Fu for giving me the mentorship, guidance, and opportunity to learn and grow in the lab.

I'd like to thank Dr. Tristan Shi and Dr. Dan Fu for their feedback and commentary on the completion of this work.

I. Background

1.1 Stimulated Raman Scattering

Raman spectroscopy has long been used to identify molecules by their characteristic vibrational frequencies, providing a chemical fingerprint.[2] However, the spontaneous Raman effect is inherently weak, limiting its use in imaging applications where speed and sensitivity are critical.[3] Stimulated Raman scattering (SRS) overcomes this by using two coherent laser fields to coherently drive a vibrational transition, improving signal intensity by up to 10^8 over its spontaneous counterpart.

To understand how SRS works we must begin with the quantum states of molecules. Initially most molecules begin at their ground state.[4] In a stimulated Raman process the molecule is then simultaneously struck by two wavelengths of light: the pump and Stokes photons. The photon energy difference between the pump and Stokes beam matches the vibrational frequency of a specific molecular bond. First the pump excites it into a virtual excited state, then it relaxes into a specific vibrational state other than the ground state as shown in Figure 1.1.[1] The Stokes beam provides a coupling between the initial ground state and final vibrational state that the molecule relaxes into. Each photon that undergoes these transitions is shifted from the pump frequency to the Stokes frequency. This shift is then detected as stimulated Raman loss or gain.

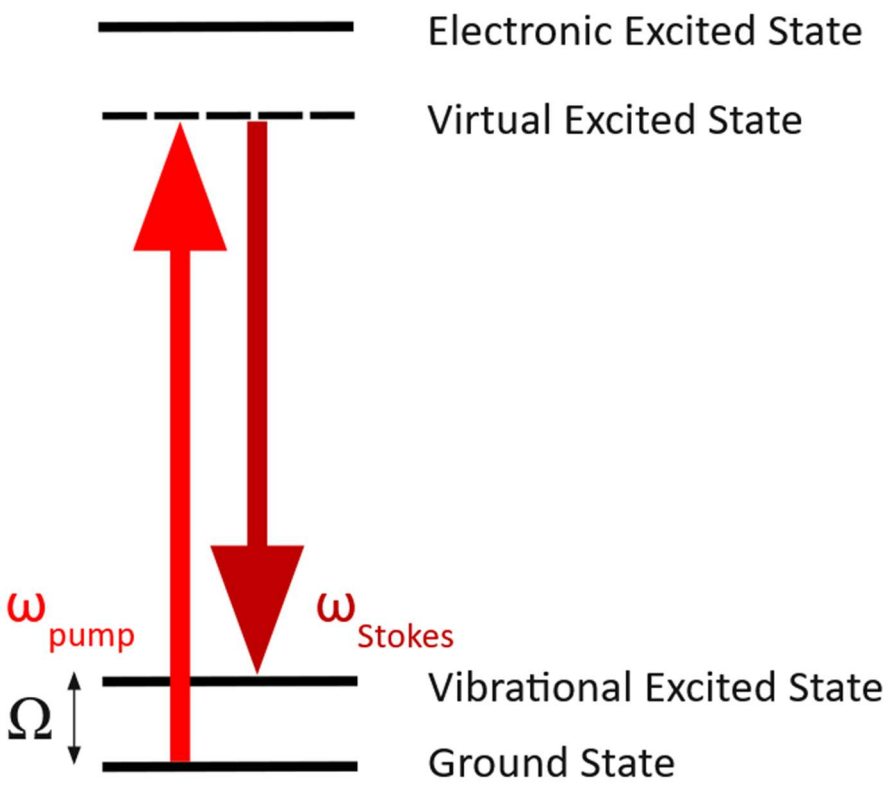

Figure **1.1** Energy level diagram for a stimulated Raman scattering process.

In SRS microscopy, the pump and Stokes beams are tuned to a specific known vibrational transition that can be observed in the sample. For example, cell imaging is commonly done with frequencies that probe lipids, proteins, or nucleic acids vibrational states.[4,5] This allows for selective and label free identification of various parts of cells.

1.2 Laser Scanning Microscopy

Laser scanning microscopy is an advanced optical imaging technique that enables high-resolution, three-dimensional visualization of biological and material specimens with exceptional spatial precision. Unlike conventional widefield microscopy, which illuminates the entire sample simultaneously, a laser scanning microscope illuminates only a single

diffraction-limited point at a time. This is achieved by focusing a coherent laser source to a discrete focal point within the specimen. The result is a significant improvement in axial resolution and optical sectioning capability.[6]

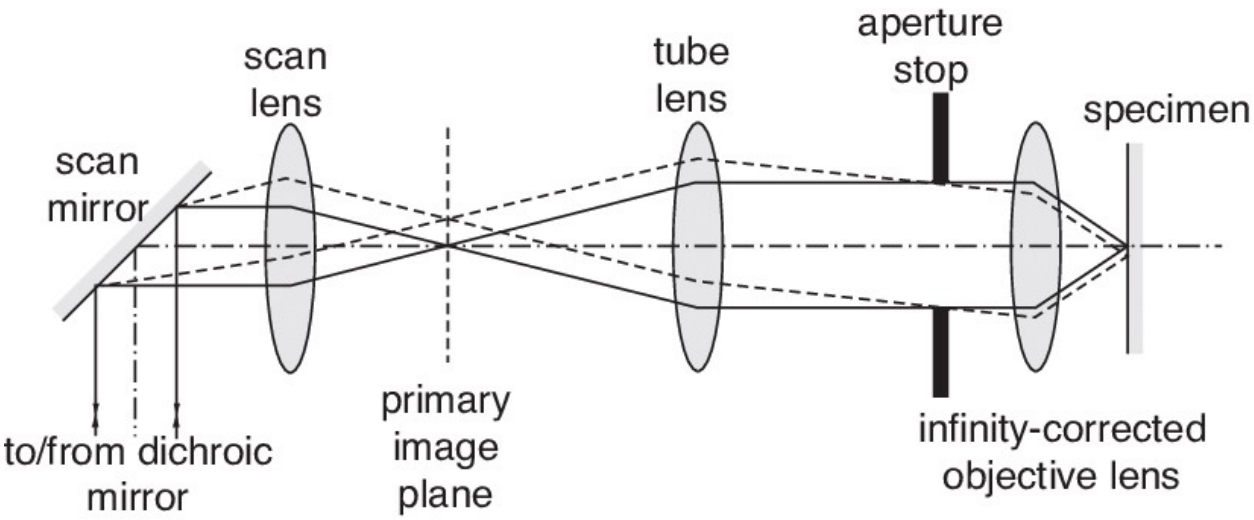

Figure **1.2** A lens diagram of the laser scanning confocal microscope.[6]

The laser beam in a laser scanning microscope is directed through a pair of galvanometric scanning mirrors, which deflect the beam rapidly and precisely along the lateral x- and y-axes of the specimen plane as shown in Figure 1.2. These galvo mirrors enable point-by-point raster scanning across the field of view, with the beam position at any given moment corresponding to a single pixel in the resulting image. Following the scanning mirrors, the beam passes through a scan lens, which collimates the angularly deflected rays into a set of parallel beams, and subsequently through a tube lens, which focuses those beams to a diffraction-limited spot at the back focal plane of the objective. Together, the scan lens and tube lens form a telescope that ensures the beam pivots about the back aperture of the objective regardless of scan angle, maintaining uniform illumination and resolution across

the entire field. The sequential acquisition of signal at each scanned point is then reconstructed computationally to form a high-fidelity two-dimensional image.

1.3 Chromatic Aberration

Light crossing an interface between two media of differing refractive indices changes direction according to Snell's law:

$$n_1 \sin(\theta_1) = n_2 \sin(\theta_2)$$

The refractive index of a material is given by:

$$n(\lambda) = A + \frac{B}{\lambda^2} + \frac{C}{\lambda^4}$$

We can see from these equations that the refractive index in Snell's law differs according to the wavelength of light incident to the transition between the media. This results in a wavelength-dependent an angular shift in focal point when light of varying wavelengths is focused through a lens. This is broadly termed chromatic aberration, but there are multiple forms of chromatic aberration observed in lens systems. The first is chromatic focal shift. Chromatic focal shift is a phenomenon where on axis rays of longer wavelengths are focused

farther as shown in Figure 1.3.

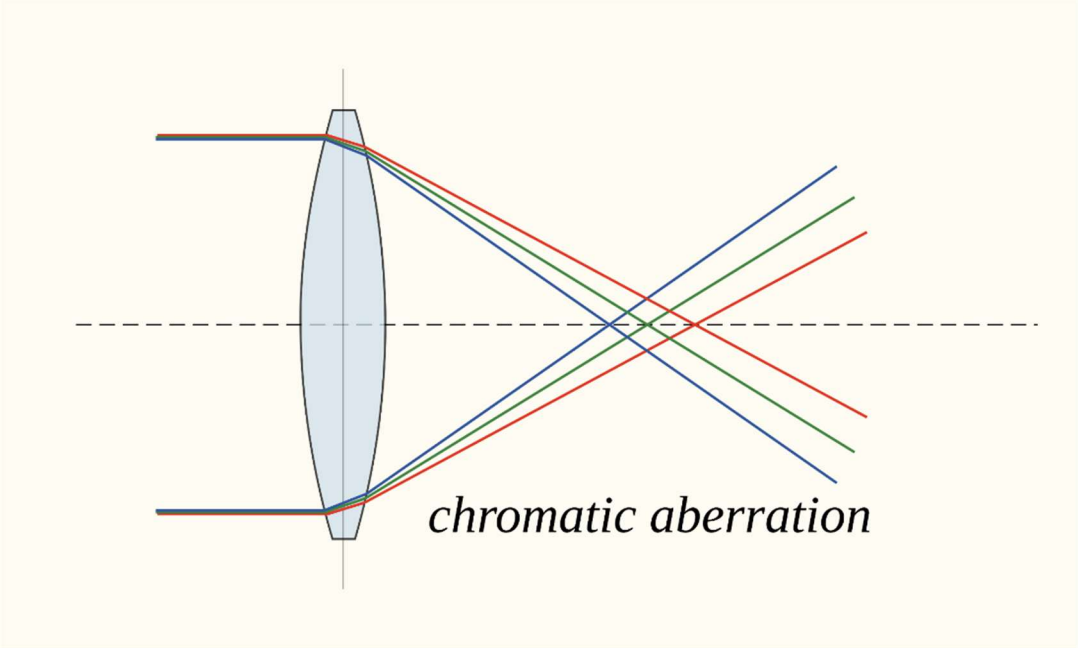

Figure **1.3** A ray diagram of various wavelengths of light traveling through a lens.[7]

The second type of chromatic aberration relevant to discuss is lateral color. Lateral color aberration occurs when off-axis rays of different wavelengths are refracted by different amounts, causing them to arrive at the image plane at different heights. Because each wavelength is focused to a slightly different lateral position, the effective magnification of the system varies with wavelength. This means that an image formed in red light will be slightly larger or smaller than the same image formed in blue light. Thus, large incident angles have large color fringes.[8]

1.4 Chromatic Effects on Stimulated Raman Scattering

Stimulated Raman scattering is a two-photon process that requires precise spatial and temporal overlap between a pump photon and a Stokes photon at two distinct wavelengths.

As discussed in previous sections, the refractive index of optical glass is wavelength-dependent, causing lenses to focus different wavelengths at slightly different axial and lateral positions, a phenomenon known as chromatic aberration. In an SRS microscope, this mismatch in focal position between the pump and Stokes beams leads to reduced spatial overlap at the sample plane, resulting in a significant drop in SRS signal at larger field-of-view positions. This effect is illustrated in Figure 1.4, which shows an SRS image of 99% DMSO at 2913 cm^{-1} and highlights the intensity difference between the on-axis position and the maximum field position.

The severity of this chromatic mismatch scales with the separation between the pump and Stokes wavelengths and the field angles incident to the imaging system. At larger scan angles, off-axis rays experience greater differential refraction, compounding the spatial walk-off between the two beams. This means that while on-axis SRS images may have a large signal to noise ratio, the same sample imaged at the periphery of the field will exhibit artificially reduced signal intensity that does not reflect the true chemical concentration. Correcting for this aberration, through optical design and the use of specialized achromatic lenses, is therefore an important consideration when gathering SRS images.

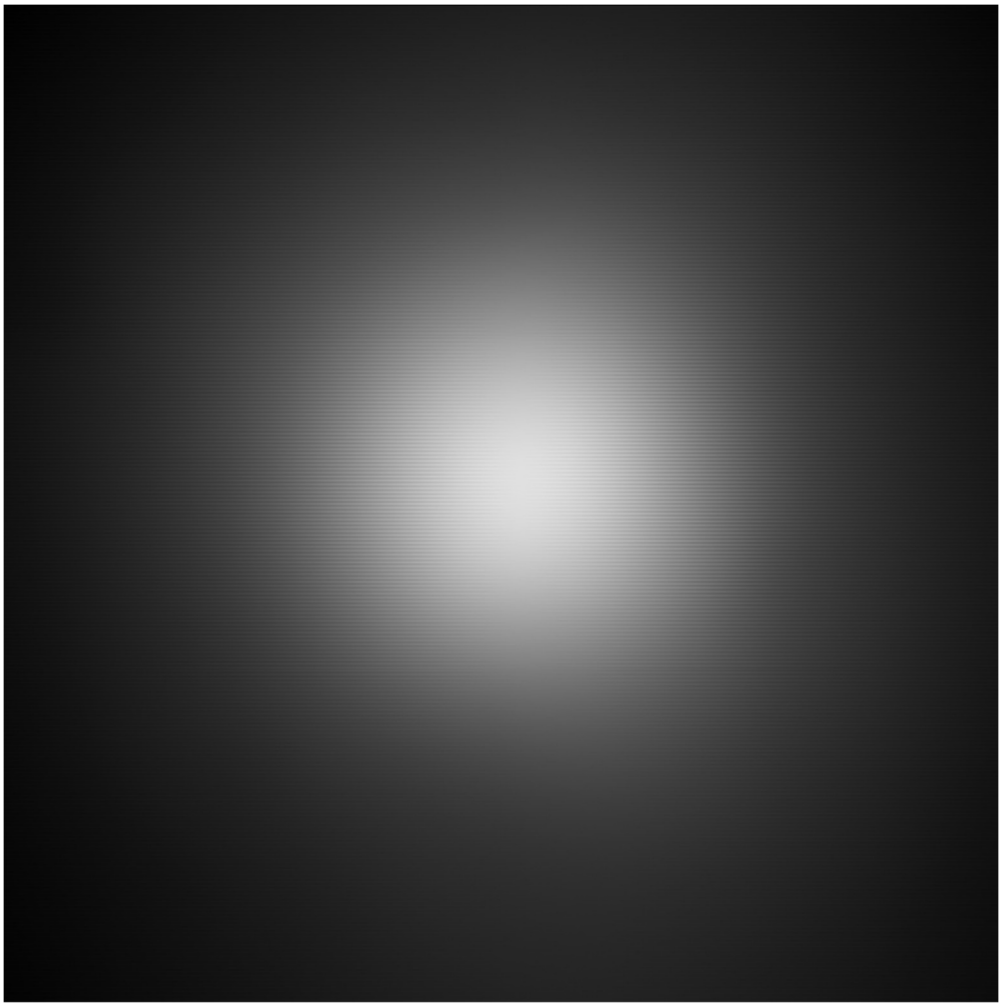

Figure **1.4** An SRS Image of 99% Dimethyl Sulfoxide at full field of view. Image Courtesy of Brian Wong.

1.5 The Achromatic Doublet

The simplest optical solution to chromatic aberration is the achromatic doublet lens, which consists of a convex crown glass element cemented to a concave flint glass element as shown in Figure 1.4. The convex crown glass element performs the primary focusing function but in doing so introduces chromatic aberration, as its refractive index varies with

wavelength and therefore focuses different wavelengths at slightly different axial positions.[9] The cemented flint glass element has a stronger dispersion and opposite curvature, such that the chromatic error introduced by the crown element is partially cancelled, bringing two selected wavelengths to a common focal point.

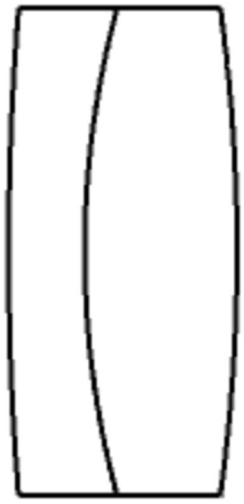

Figure **1.5** A lens diagram of an achromatic doublet.

However, the achromatic doublet has several limitations. First, the design only corrects chromatic aberration at exactly two wavelengths, which are chosen by the lens designer. For any other wavelengths within the passband, a residual chromatic error remains. This means that unless the pump and Stokes wavelengths used in an SRS experiment coincide precisely with the two corrected wavelengths of the doublet, some degree of chromatic mismatch will persist. Second, a single achromatic doublet produces significant pincushion distortion at high field angles. This geometric distortion arises from the variation in magnification across the field of view and is not addressed by the achromatic design, which targets only chromatic correction. As a result, images acquired with a single achromatic doublet as the scan or tube

lens will exhibit both residual chromatic aberration and geometric warping at the periphery of the field.

1.6 The Plössl Eyepiece

A more effective optical solution for correcting chromatic aberration is the Plössl eyepiece design, which consists of two achromatic doublets arranged symmetrically and facing in opposite directions as shown in Figure 1.5. This configuration retains all the chromatic correction benefits of a single achromatic doublet but distributes the refractive work across four lens elements rather than two. As a result, the chromatic aberration introduced by the first doublet is partially corrected by that doublet itself and further corrected by the second, reducing the residual secondary spectrum and bringing the final chromatic performance beyond what a single doublet can achieve.

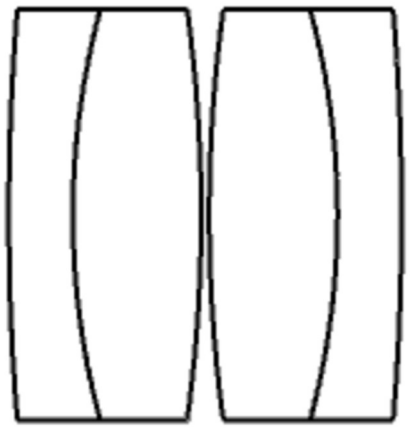

Figure **1.6** A lens diagram of a Plössl eyepiece of achromatic doublets.

The symmetric arrangement of the Plössl design also provides a significant advantage in terms of geometric distortion. In a single achromatic doublet, pincushion distortion accumulates without any compensating element to counteract it. In the Plössl configuration, the two doublets are oriented in opposition such that the pincushion distortion generated by the first doublet is largely cancelled by the barrel distortion introduced by the second. This mutual cancellation arises naturally from the symmetry of the design and means that the Plössl eyepiece produces substantially lower geometric distortion across the field of view compared to a single doublet. These combined benefits make the Plössl a practical and cost-effective choice for SRS microscopy.

The 2x Thorlabs AC-254-100-B Plössl eyepiece configuration was shown to be the best cheap commercial option in a paper published in 2014 by Negrean Et Al.[10] They found chromatic focal shift, lateral color, and F-theta distortion were minimized compared to single achromats. This project attempted to move past the standard configuration shown in 2014, to improve chromatic performance to a level where larger field of views can be imaged with strong SRS signal.

II. Experimental Methods

2.1 Imaging Procedure

To quantify chromatic aberration across the field of view, a 99% DMSO solvent sample was used as a reference standard, as its strong and well-characterized Raman signal provides a reliable benchmark for assessing spatial signal uniformity. Before imaging, the microscope system was verified to be properly aligned using the following procedure. A slide of 99% DMSO was placed under the microscope and observed under bright field illumination, and the condenser and objective were focused on the correct axial depth. The pump and Stokes beams were then spatially aligned through the scan lens and tube lens, and the modulation of the Stokes beam was verified using an oscilloscope. The collimation of both beams through the objective and condenser was subsequently checked and corrected as needed. Finally, the focusing lens pair was aligned to the photodiode and a DC signal was confirmed. Once a DC signal was observed, temporal delay and spatial alignment were adjusted to maximize SRS. The resulting SRS image from this procedure is shown in Figure 1.3. Taking SRS images using the procedure above does not quantify chromatic aberration however, so the next step in the imaging process is imaging a Thorlabs R1L3S30C1 negative target grid independently with the pump and Stokes beams. The imaging procedure from the previous paragraph is carried out, and then one of the beams is blocked and a 1-micron step size Z-stack image of the target grid is recorded as shown in Figure 2.1. The two independent Z stacks with different wavelengths allows us to quantify focal plane changes between the two.

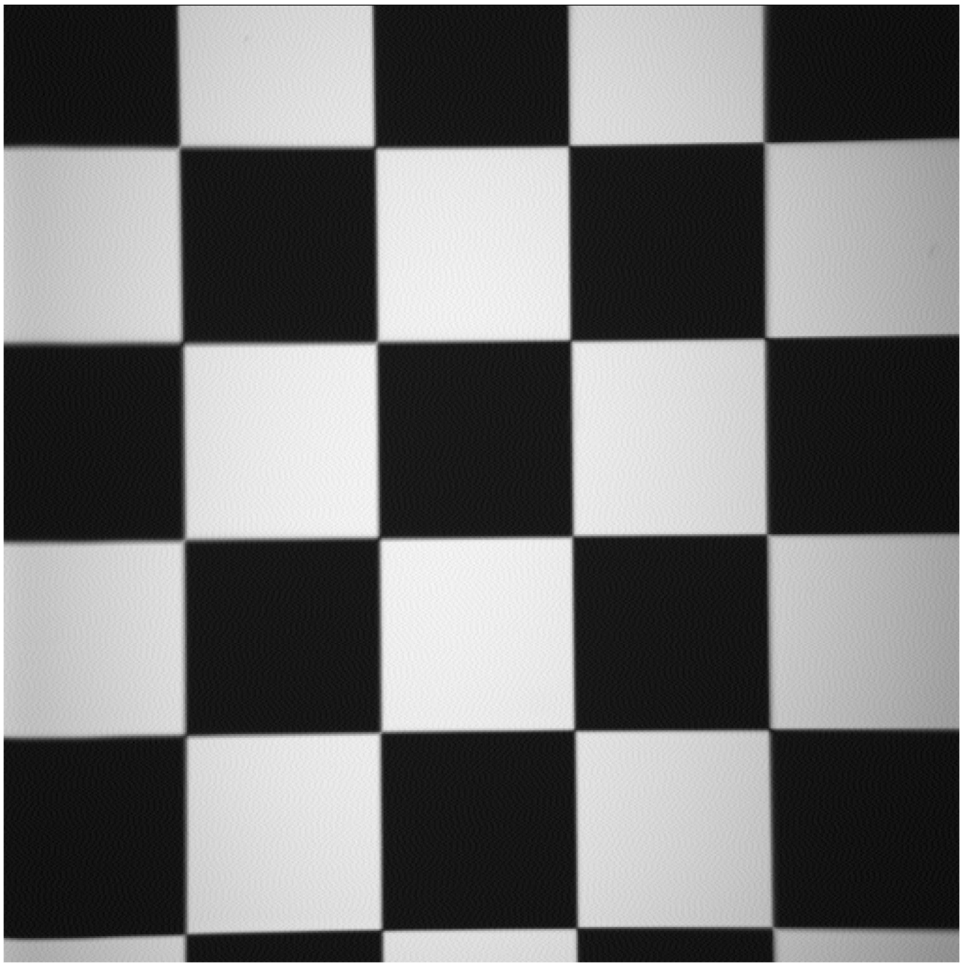

Figure **2.1** A laser scanning image of a Thorlabs R1L3S30C1 negative target grid.

2.2 Measurement of Chromatic Focal Shift

Chromatic focal shift refers to the axial displacement in focus position between light of different wavelengths, arising from the wavelength-dependence of the refractive index in the lens elements of the optical system.[11] It is quantified as the difference in focal depth, measured in microns, between two specified wavelengths. In the context of the SRS microscope used in this work, the relevant wavelengths are the 1030 nm Stokes beam and the 793 nm pump beam. Because SRS signal generation requires precise axial overlap between

these two beams at the focal plane, any axial displacement between their respective focal positions will reduce the efficiency of the stimulated Raman process and degrade image quality. Measuring the chromatic focal shift between these two wavelengths therefore provides a direct and quantitative assessment of one of the primary sources of signal loss in the system.

The data analysis pipeline for producing chromatic focal shift measurements was as follows. The Z stack images were imported into Python, and 100 horizontal and vertical lines were drawn across each image to create a dense grid, as shown in Figure 2.2.

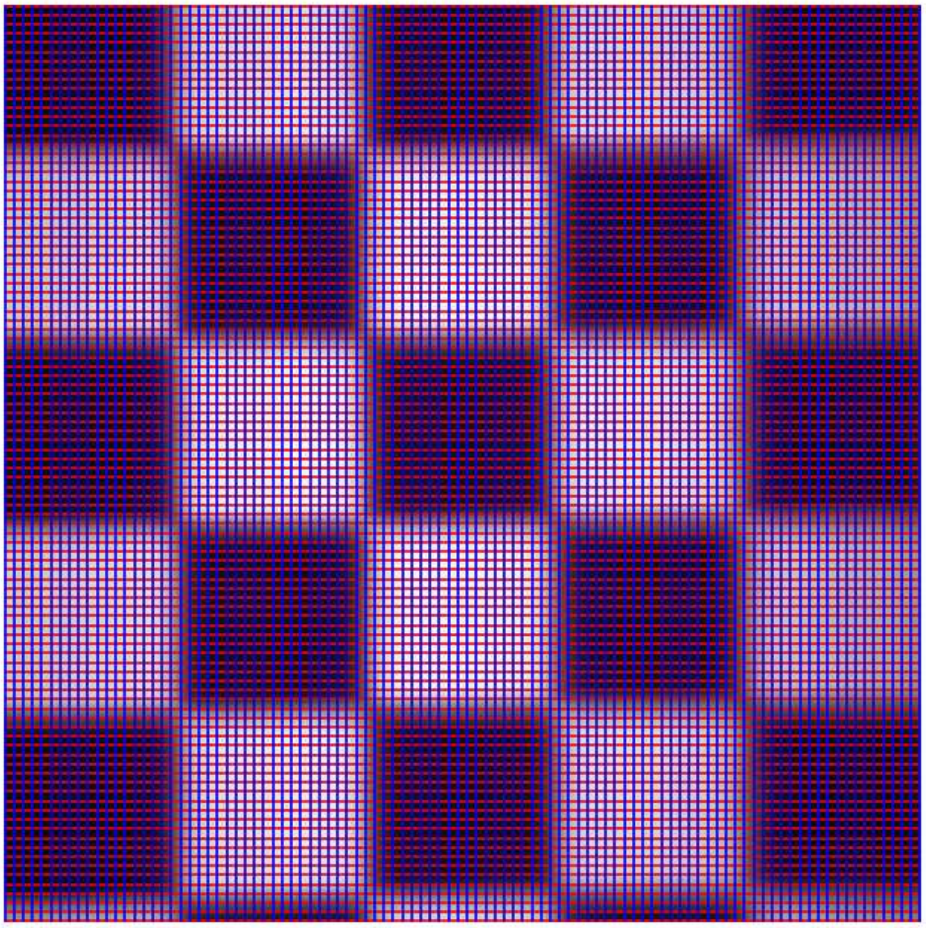

Figure **2.2** A laser scanning image of a Thorlabs R1L3S30C1 negative target grid with 100x100 vertical and horizontal lines drawn over it.

Following the construction of the grid, the derivative of the pixel intensity values was computed along each line and recorded. This produced a plot displaying peaks at locations where transitions between dark and light pixels occurred, corresponding to the edges of the grid features. An example of this derivative plot is shown in Figure 2.3.

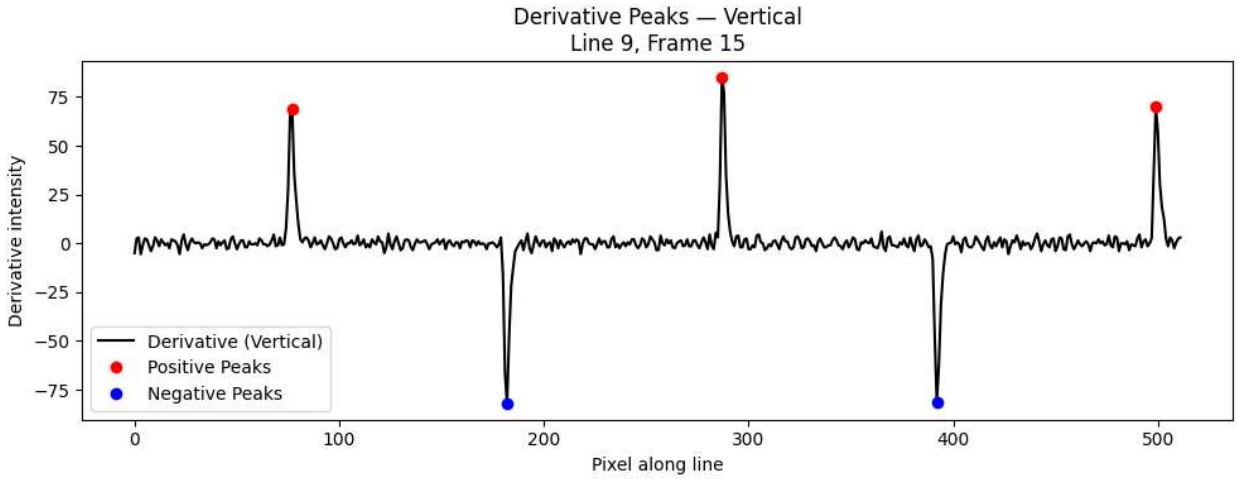

Figure **2.3** A line plot of the derivative of the pixel values of the Thorlabs grid image across horizontal line 9 on frame 15.

The full width half maximum (FWHM) of these peaks defines the sharpness of the transition from light to dark or dark to light. This provides a quantitative metric for

determining the precise axial depth at which each region of the image is most sharply focused.

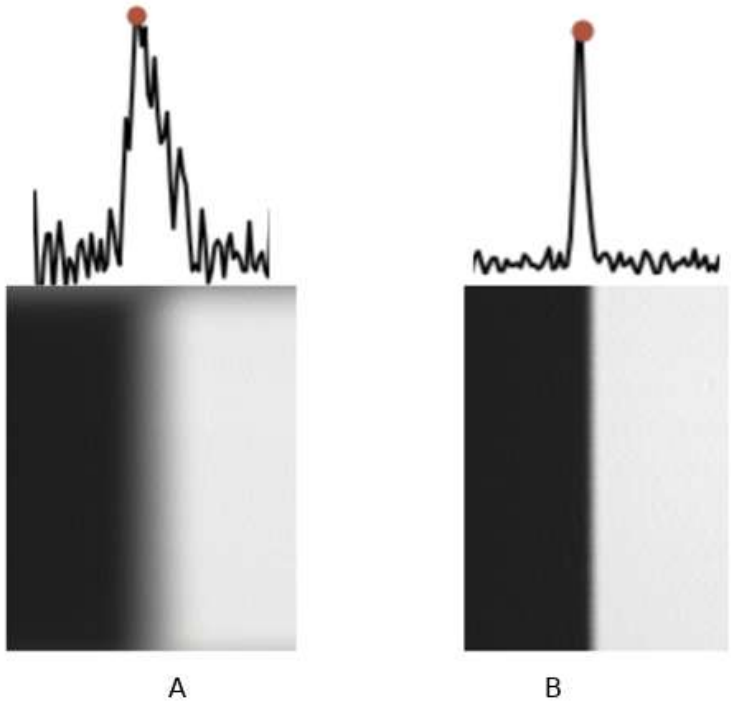

Figure **2.4 (A)** A peak on a line plot from a very out of focus frame of the Thorlabs grid image. **(B)** A peak on a line plot from a very in focus frame of the Thorlabs grid image.

After fitting a Gaussian FWHM to each peak, a most in focus frame is fed to the program from visual inspection of the data and it iteratively moves outward from that in focus frame to find the minimum FWHM. This is recorded as the most in focus frame. The result is a grid of points where each point represents a Z value of best focus.

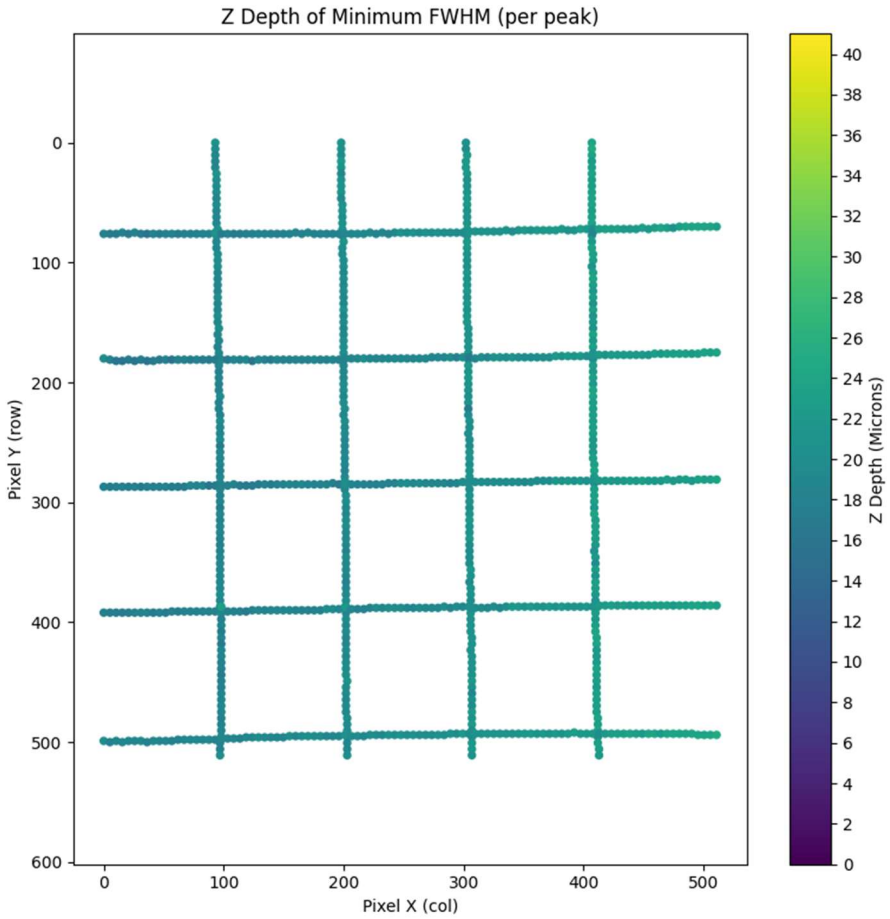

Figure **2.5** A 2D scatter plot of the peak positions of the derivative profiles across the 100x100 lines drawn on the grid image. Where X and Y axes are the peak position, and color is the Z depth of the frame.

This plot shows just the focal depth of the image for one wavelength of light. To quantify chromatic aberration, we need to find the Z difference between the two wavelengths, so this plot is produced for each wavelength, and then points are paired and the Z values are subtracted to get a ΔZ between the two. The average ΔZ was computed by finding the mean

frame difference over all total points, and this gives us the average chromatic focal shift plotted in Figure 2.6.

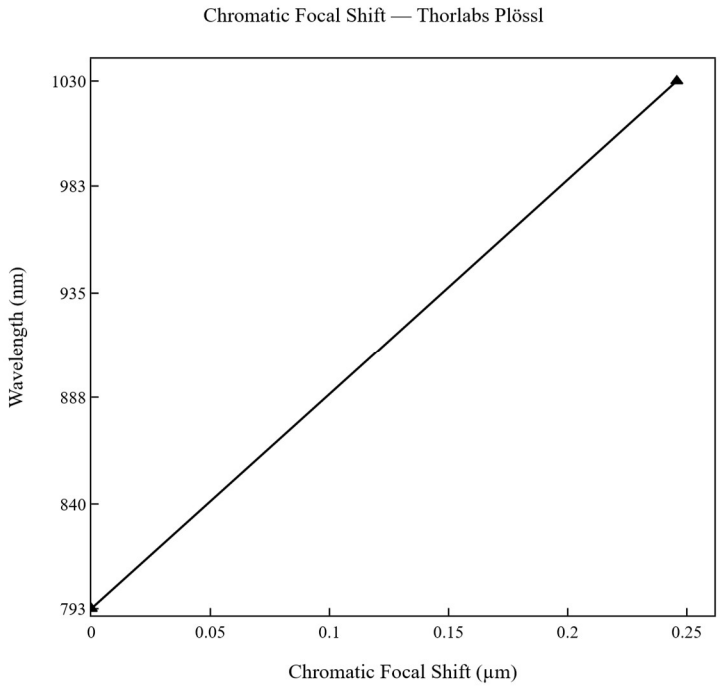

Figure **2.6** A line plot of chromatic focal shift in microns vs wavelength in nanometers.

2.3 Measurement of Lateral Color

Lateral color aberration refers to the variation in magnification between light of different wavelengths across the field of view. Unlike chromatic focal shift, which manifests as an axial displacement between wavelengths, lateral color produces a lateral displacement that increases with distance from the optical axis. In practice this means that the same object will be imaged at slightly different sizes depending on the wavelength of light used, with the two images appearing coincident at the center of the field but progressively diverging toward the

periphery. In the SRS microscope, this means the pump and Stokes beams will sample slightly different lateral positions at large field angles, reducing their spatial overlap and contributing to the signal roll-off observed across the field of view.

To quantify this effect the positions of the grid points were extracted and plotted as shown in Figure 2.7. By overlaying the grid point maps from the two wavelengths, any difference in the spatial distribution of the grid points can be attributed to lateral color aberration.

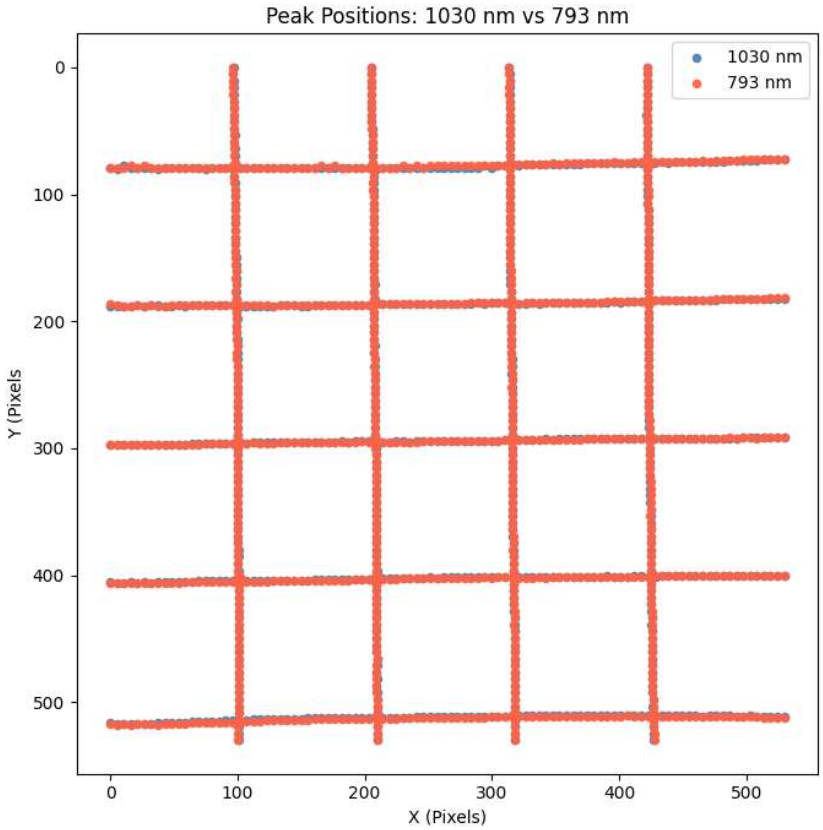

Figure **2.7** A 2D scatterplot of the grid intersections from the 1030 nm image and 793 nm image overlaid.

Each point can now be paired with its closest neighbor of the other wavelength, and the distance formula:

$$d = \sqrt{(x_2 - x_1)^2 + (y_2 - y_1)^2}$$

can be used to calculate the lateral color difference between individual points. This lateral color difference of individual points should increase as field height increases. Since pixels in the image correspond to a precise angle of the horizontal and vertical galvo mirrors, we can convert our pixels to x and y scan angles and average over each line to get x and y lateral color as a function scan mirror angle.

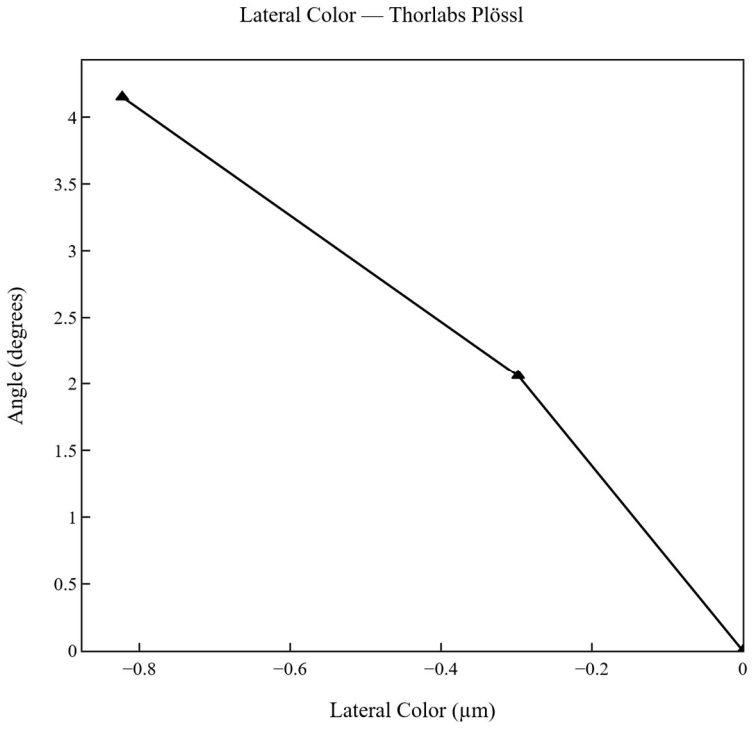

Figure **2.8** A line plot of lateral color vs scan mirror angle.

2.4 Simulation of the Microscope Lens System

To contextualize empirical measurements made in the previous section, the following section presents a Zemax OpticStudio simulation of the lens system, from which theoretical chromatic aberration can be derived and compared against the experimental results. The simulation incorporates the three primary optical elements of the system: the scan lens, tube lens, and objective. The objective was modeled as a perfect lens, and the Thorlabs TTL-200-B lens was modeled with a black box model provided by Thorlabs. The initial lens configuration is shown in Figure 2.9. We can see a Plössl eyepiece with two Thorlabs AC-254-100-B lenses giving an effective focal length of 50 mm, followed by the Thorlabs TTL-200-B and finally our perfect paraxial objective. The source was modeled with our two wavelengths 1030 and 793 nm and an entrance pupil of +-5 degrees.

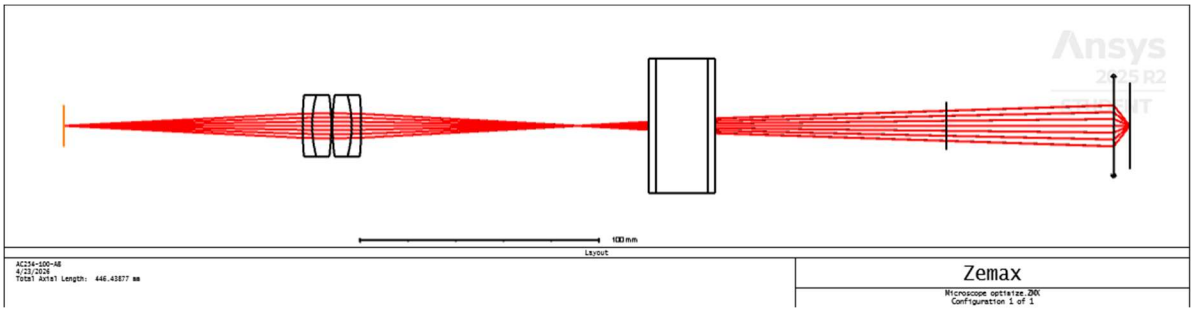

Figure **2.9** A layout diagram of the scan lens tube lens and objective microscope system in Zemax OpticStudio

2.5 Chromatic Performance Optimization

Zemax OpticStudio provides a wide range of aberration metrics for characterizing the optical performance of lens systems. Of these, the two most relevant to this work are

chromatic focal shift and lateral color aberration, as described in Sections 2.2 and 2.3. To improve the performance of the simulated optical system with respect to these metrics, the built-in optimization framework in Zemax OpticStudio was employed.

Optical system optimization in Zemax OpticStudio is an iterative numerical process, as no analytical solution exists for the ideal lens configuration in a given application.[9] The optimization is guided by a merit function, which is a scalar quantity that aggregates the contributions of multiple performance criteria including spot size, aberration, distortion, wavefront error, and any additional constraints specified by the designer. Optimization proceeds by allowing the routine to vary a defined set of lens parameters, such as surface curvatures, thicknesses, or glass types, while tracing rays through the system and adjusting those parameters iteratively until the merit function is minimized. This process is repeated across multiple cycles until further adjustment of the variables produces no significant reduction in the merit function.[12]

Optimization was carried out by performing a quick focus adjustment on the scan lens distance. Then the merit function was edited to optimize thicknesses of the air spacing between lenses, with the constraint that no thickness can go above the 170 mm max pupil distance of the TTL-200-B. This resulted in the final lens system in Figure 2.9.

2.6 Selecting a New Lens System

A comparison of over 20 commercial lens configurations was conducted in Zemax OpticStudio, with chromatic focal shift and lateral color aberration recorded for each. The configurations tested included individual achromatic doublets from multiple manufacturers, matched Plössl eyepiece pairs, non-matching Plössl eyepiece combinations, and doublet-

singlet eyepiece arrangements. Figure 2.10 shows representative examples of the configurations evaluated.

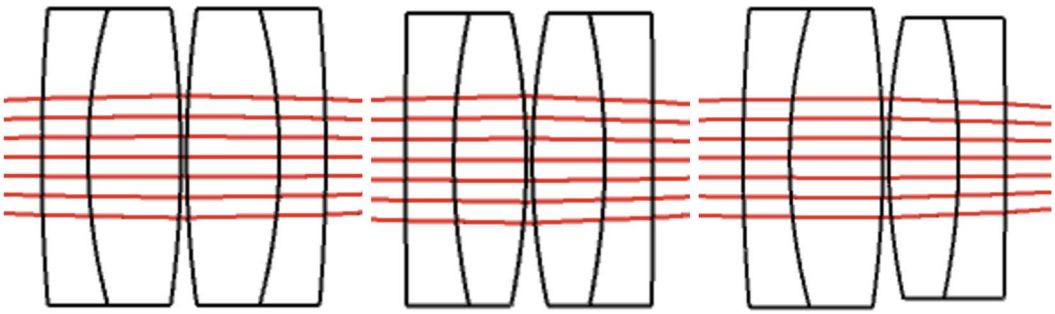

Figure **2.10** Three Plössl eyepieces with incident rays traced.

Of the configurations tested, two candidates stood out from the rest. The configuration exhibiting the lowest overall chromatic aberration was a Plössl eyepiece consisting of two Edmund Optics NIR I coated achromatic doublets with a 100 mm focal length. This configuration produced nanometer-level lateral color and a chromatic focal shift of 0.2 um. The configuration that most effectively corrected the lateral color aberration present in the system was a Plössl eyepiece consisting of two Newport Scientific PAC12AR.16 100 mm focal length achromatic doublets, which produced a maximum lateral color of 0.216 um at a normalized field angle of 0.72. This represents a theoretical correction of approximately 60% of the lateral color measured in the Thorlabs test grid images at that field angle. Given the strong simulated performance of both candidates relative to the other configurations evaluated, both were procured for experimental validation.

III. Results and Discussion

3.1 Thorlabs Lenses

Having established the data analysis workflow and validated its performance with the baseline optical configuration, we now turn to a systematic comparison of different lens systems. The following discussion evaluates how well the workflow can detect and quantify differences in optical performance between configurations of varying quality, using chromatic focal shift and lateral color as the primary metrics.

From Negrean et al., the Thorlabs AC254-50-B achromatic doublet lens is known to exhibit poor chromatic performance and high F-theta distortion relative to purpose-built scan lenses.[10] This makes the lens a natural candidate for testing the sensitivity of the analysis workflow: by substituting the AC254-50-B for the baseline scan lens and repeating the characterization procedure, any degradation in optical performance should be clearly

reflected in the output metrics. Figures 3.1 3.2 and 3.3 show the chromatic performance of the AC254-50-B compared with our Plössl eyepiece.

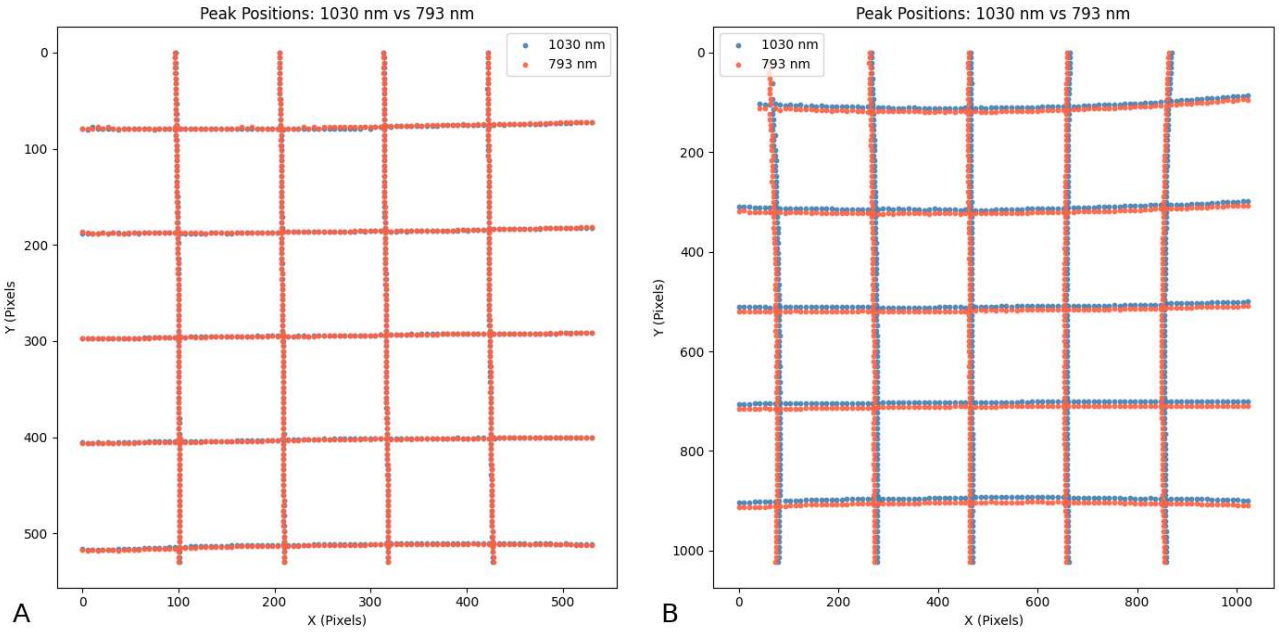

Figure **3.1 (A)** A 2D scatterplot of the grid intersections from the Thorlabs Plössl eyepiece 1030 nm image and 793 nm image overlaid. **(B)** A 2D scatterplot of the grid intersections from the Thorlabs Achromat 1030 nm image and 793 nm image overlaid.

Across all metrics, the AC254-50-B configuration performs significantly worse than the baseline scan lens. Large F-theta distortion is visible at the edges of the field, and lateral color is clearly present at all grid line intersections. The lateral color and chromatic focal shift were quantified in Figure 3.2. A standard Thorlabs Plössl eyepiece produced visibly reduced chromatic aberration compared to the AC254-50-B.

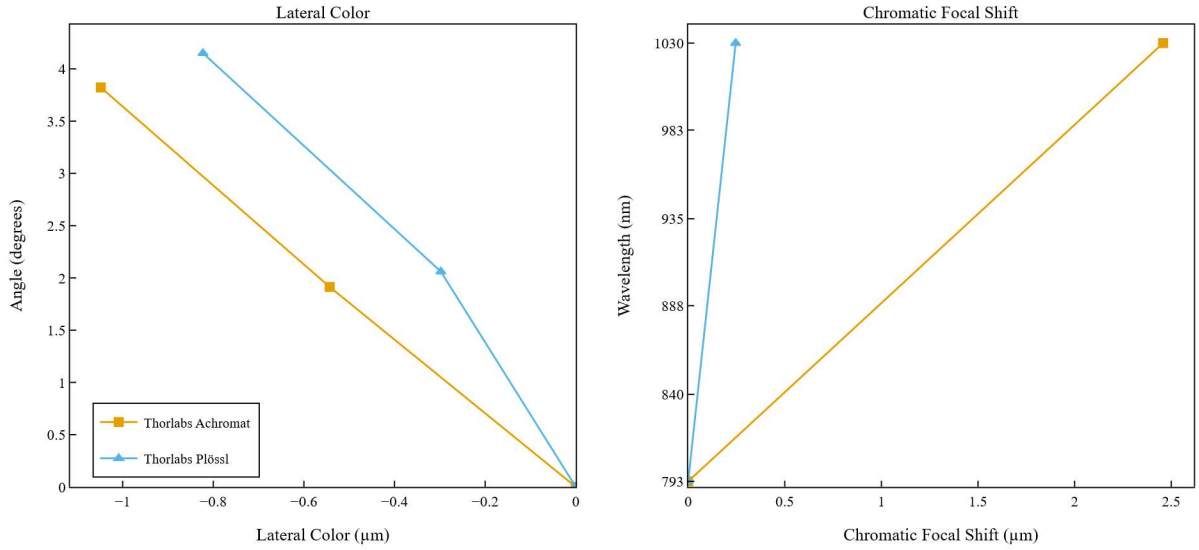

Figure **3.2** Line plots of aberration metrics for a Thorlabs AC-254-50-B Scan Lens compared to a Thorlabs Plössl eyepiece.

This confirms that the data analysis pipeline can detect aberrations caused by scan lens changes. We see a 10x increase in chromatic focal shift, and 4x increase in lateral color.

3.2 Newport Scientific Lens

The next test examined whether the lateral color could be corrected by substituting the Newport Scientific PAC12AR.16 as the scan lens. Zemax simulation of the Newport lens indicated it had slightly positive lateral color which could correct for the negative lateral color measured in the system before. This made it an ideal candidate for testing alignment between simulation and reality. The same imaging procedure and analysis pipeline were applied, with the results shown in Figures 3.3 and 3.4.

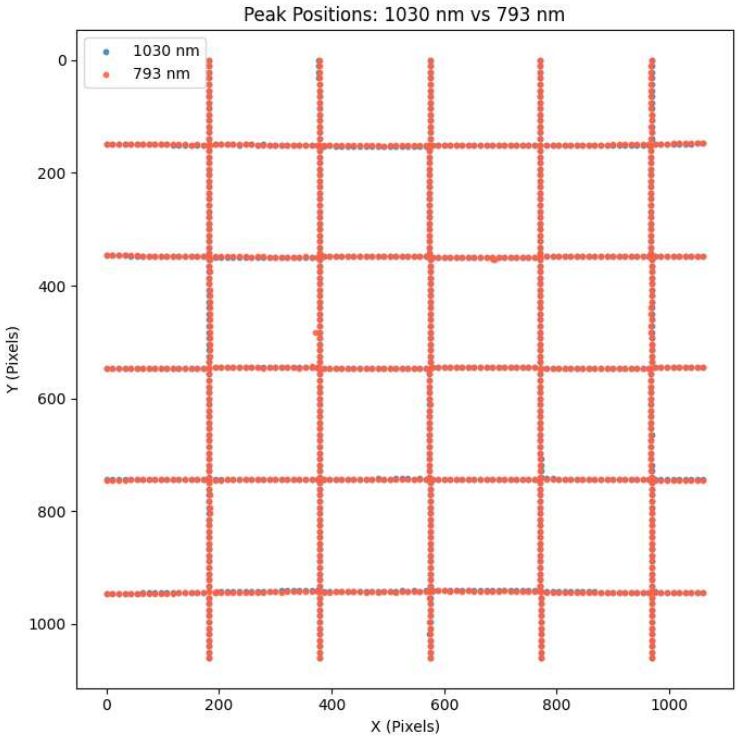

Figure **3.3** A 2D scatterplot of the grid intersections from the Newport Scientific Plössl eyepiece 1030 nm image and 793 nm image overlaid.

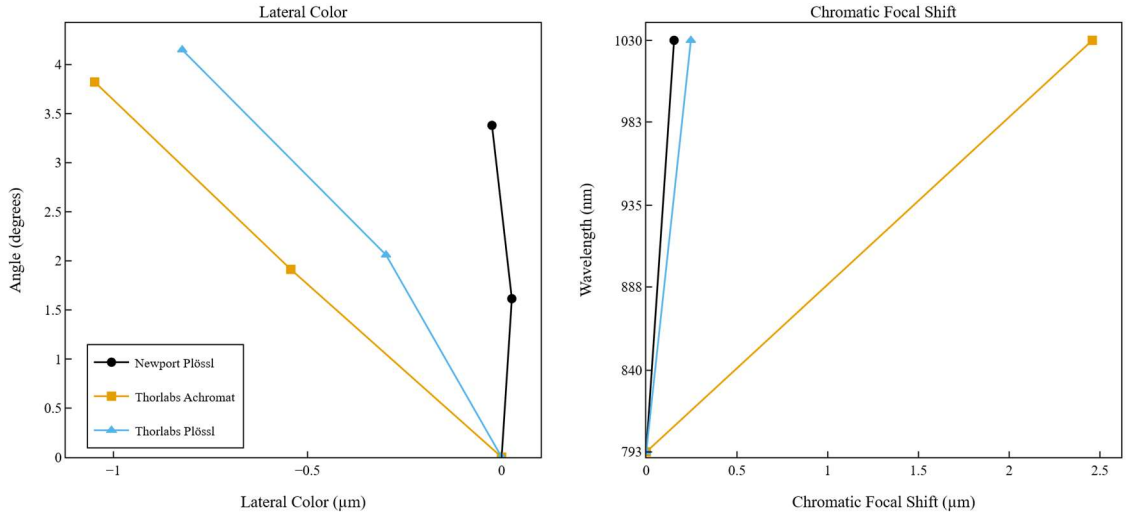

Figure **3.4** Line plots of aberration metrics for a Newport Scientific Plössl eyepiece compared with a Thorlabs Plössl eyepiece and Thorlabs achromatic doublet.

The Newport Scientific Plössl eyepiece demonstrated significant improvements in lateral color and F-Theta distortion, with a modest improvement in chromatic focal shift as well. At high field angles, the lens effectively corrected for lateral color aberration, reducing the average lateral color difference to sub pixel levels. SRS imaging of 99% DMSO with the new scan lens configuration as seen in Figure 3.5 showed substantially increased signal at higher scan angles, expanding the viable field of view for cell imaging. The previous DMSO images like Figure 1.4 show just how large an improvement the scan lens change has caused. We see

an increase in FWHM of the intensity profile plot of just under 200 microns. This is a 2.7 fold increase in usable imaging area.

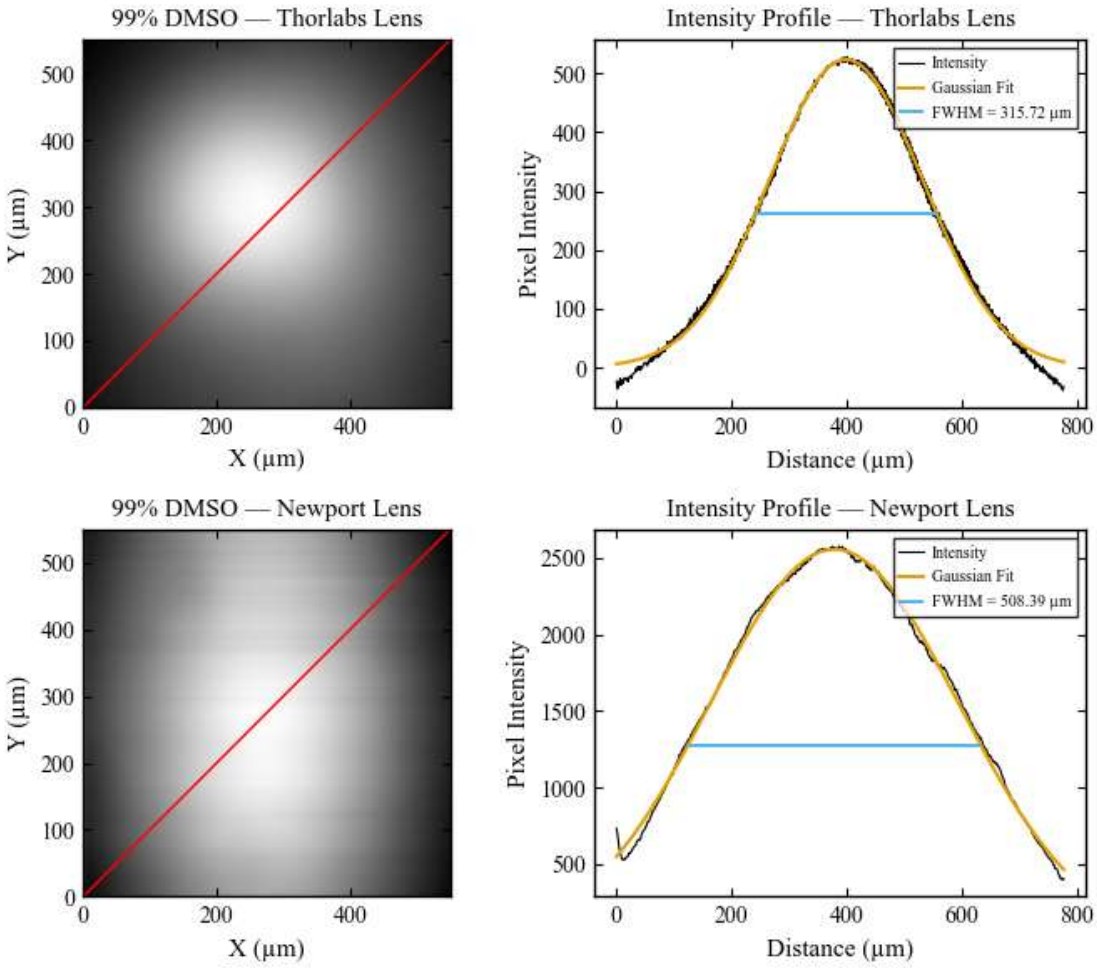

Figure **3.5** A comparison of SRS images taken with the Thorlabs Scan Lens and Newport Scan Lens

IV. Conclusion

4.1 Conclusion

This work addressed a limitation in stimulated Raman scattering microscopy: the degradation of signal at large field angles caused by chromatic aberration in the scan lens system. By developing a quantitative characterization pipeline based on Z-stack imaging of a calibration grid, chromatic focal shift and lateral color aberration were measured directly and reproducibly across multiple lens configurations. The workflow proved sensitive enough to detect meaningful differences between configurations, capturing the expected performance gap between a single achromatic doublet and a Plössl eyepiece arrangement.

Building on this characterization framework, a systematic comparison of over twenty commercial lens configurations was conducted in Zemax OpticStudio. A Plössl eyepiece of Newport Scientific PAC12AR.16 100 mm focal length achromatic doublets emerged as the strongest candidate for lateral color correction, and experimental validation confirmed the simulation results. The new configuration reduced the average lateral color difference to sub pixel level at high field angles and produced substantially increased SRS signal at large scan angles compared to the baseline Thorlabs configuration. This translated directly into improved image uniformity across the field of view, expanding the range of scan angles at which reliable cell imaging can be performed.

Taken together, these results demonstrate that careful optical characterization and lens selection can meaningfully improve SRS microscope performance without requiring custom optics. The characterization pipeline developed here is general and could be applied to future lens evaluations as improved commercial options become available, or as the system is adapted for new wavelength combinations. Continued work in this direction, particularly

toward designing a custom scan lens to fit the system's needs, may further extend the usable field of view and bring the system closer to diffraction-limited performance across the full scan range.

References

(1) Freudiger, C. W.; Min, W.; Saar, B. G.; Lu, S.; Holtom, G. R.; He, C.; Tsai, J. C.; Kang, J. X.; Xie, X. S. Label-Free Biomedical Imaging with High Sensitivity by Stimulated Raman Scattering Microscopy. *Science* **2008**, *322*, 1857–1861.

(2) Raman, C. V.; Krishnan, K. S. A New Type of Secondary Radiation. *Nature* **1928**, *121*, 501–502.

(3) De Luca, A. C.; Mazilu, M.; Riches, A.; Herrington, C. S.; Dholakia, K. Stimulated Raman Scattering Microscopy in Chemistry and Life Science. *Chem. Soc. Rev.* **2016**, *45*, 1844–1858. https://doi.org/10.1039/C5CS00693G

(3) Atkins, P. W.; de Paula, J. *Physical Chemistry*, 10th ed.; Oxford University Press: Oxford, 2014; pp [560–575].

(4) Xu, F. X.; Ioannou, G. N.; Lee, S. P.; Savard, C.; Horn, C. L.; Fu, D. Discrimination of Lipid Composition and Cellular Localization in Human Liver Tissues by Stimulated Raman Scattering Microscopy. *J. Biomed. Opt.* **2024**, *29* (1), 016008. https://doi.org/10.1117/1.JBO.29.1.016008

(5) Lu, F.; Basu, S.; Igras, V.; Hoang, M. P.; Ji, M.; Fu, D.; Holtom, G. R.; Neel, V. A.; Freudiger, C. W.; Fisher, D. E.; Xie, X. S. Label-Free DNA Imaging in Vivo with Stimulated Raman Scattering Microscopy. *Proc. Natl. Acad. Sci. U.S.A.* **2015**, *112* (37), 11624–11629. https://doi.org/10.1073/pnas.1515121112

(6) Sheppard, C.; Rehman, S. Confocal Microscopy. In *Biomedical Optical Imaging Technologies*; Springer-Verlag: Berlin, Heidelberg, 2013; pp 213. https://doi.org/10.1007/978-3-642-28391-8_6

(7) Mellish, B. Chromatic Aberration Diagram. Wikimedia Commons, 2006. https://commons.wikimedia.org/wiki/File:Lens6b.png (accessed May 12th, 2026).

(8) Lateral Color Error. telescope-optics.net. http://www.telescope-optics.net/lateral_color.htm (accessed May 5, 2026).

(9) Carson, F. A. *Basic Optics and Optical Instruments*, Revised ed.; Dover Publications: New York, 2011.

(10) Negrean, A.; Mansvelder, H. D. Optimal Lens Design and Use in Laser-Scanning Microscopy. *Biomed. Opt. Express* **2014**, *5* (5), 1588–1609. https://doi.org/10.1364/BOE.5.001588

(11) Zhuang, J.; et al. Chromatic Focal Shift of Optical System Expressed by Related Wavelength Formulas. In *Optical Modeling and System Alignment*; Kahan, M. A., Sasián, J., Youngworth, R. N., Eds.; Proc. SPIE 11103; SPIE: Bellingham, WA, **2019**; p 111030W.

(12) Laikin, M. *Lens Design*, 4th ed.; CRC Press: Boca Raton, FL, **2006**.